



A VISION-BASED ANALOG METER READING METHOD FOR INSPECTION ROBOTS

JIACHENG LI^{*} HONGLEI WANG[†] XISHUO ZHU[‡] SIJIAN LIU[§] AND JUNSHENG ZHANG[¶]

Abstract. Computer vision technology has been widely applied in reading recognition of analog meters. However, it is still a challenge to quickly and accurately read various types of analog meters under different environmental conditions. We propose a fast-reading method for analog meters based on keypoint detection, which is applied to inspection robots. First, we use the YOLOv5s network to locate the analog meter. Second, the HRNet network is used to detect the keypoints of the pointer and scale on the dial. Third, an objective image quality assessment method that includes multiple indicators is established to select the optimal image for reading recognition. Finally, we calculate the reading of the analog meter based on the deflection angle of the pointer. The experiment shows that our method can accurately read the readings of analog meters, with an average reading error of 3.81%. It can be effectively applied to inspection robots to read analog meter readings.

Key words: analog meter; object detection; keypoint detection; inspection robot; reading recognition

1. Introduction. Many places that require accurate and reliable measurements, such as substations, chemical factories, water pump houses, and other similar locations, still use analog meters instead of digital ones. This is because analog meters are less affected by the electromagnetic environment and can provide more stable readings. However, a drawback of these meters is that they usually cannot send analog signals to a remote location for monitoring or analysis. Therefore, they depend on manual inspection by workers who have to read the analog meters in person [1]. With the developments of computer vision technology [2], it has become the mainstream method to use an inspection robot equipped with a camera for instrument recognition. Using computer vision to automatically read analog meters is more efficient and convenient than manual inspection. However, the images collected by the visible light cameras are easily affected by different poses, illumination changes, and complex backgrounds, which brings difficulties to reading recognition. Many researchers have explored vision-based methods for fast and stable instrument recognition by inspection robots [3-6].

Traditional methods for machine vision reading [7-8] have some drawbacks, which prevent them from being stably applied. These methods usually identify the dial area in an image by using template matching or Hough circle detection. Then they recognize the scale and pointer in the dial by using image segmentation or line detection. Finally, they read the meter based on the angle or distance between the pointer and the scale [9]. However, these methods are not suitable for inspection robots that work in complex and changing environments [10]. For example, they cannot adapt to different angles and lighting conditions because they rely on manually set parameters in the algorithm. This makes their detection robustness very poor.

In recent years, deep learning has been applied to analog meter recognition with remarkable results [11-14]. One of the key steps in analog meter recognition is instrument detection, which involves locating the instrument region in an image [15]. Huang et al. [17] employed an improved YOLOv3 network to locate the analog meter and a monocular-vision pointer reconstruction algorithm was used to read the instrument. In [18], a Faster Region-based Convolutional Network (Faster R-CNN) was used to detect the target meter and guide the camera

^{*}Beijing Technology Research Branch of Tiandi Science & Technology Co., Ltd., Beijing 100013, China; Intelligent Mine Research Institute, Chinese Institute of Coal Science (CICS), Beijing, 100013, China

[†]Beijing Technology Research Branch of Tiandi Science & Technology Co., Ltd., Beijing 100013, China; Intelligent Mine Research Institute, Chinese Institute of Coal Science (CICS), Beijing, 100013, China (Corresponding author, wanghonglei@mail.ccric.cteg.cn)

[‡]Beijing Technology Research Branch of Tiandi Science & Technology Co., Ltd., Beijing 100013, China; Intelligent Mine Research Institute, Chinese Institute of Coal Science (CICS), Beijing, 100013, China

[§]Beijing PINS Medical Co., Ltd., Beijing, 102200, China

[¶]Beijing Technology Research Branch of Tiandi Science & Technology Co., Ltd., Beijing 100013, China; Intelligent Mine Research Institute, Chinese Institute of Coal Science (CICS), Beijing, 100013, China

alignment. Then reading could be obtained after the pointer is recognized by Hough Transform. Salomon et al. [19] used a YOLOv4 target detector and proposed a new regression method (AngReg) to achieve automatic meter reading in unconstrained scenarios. Fan et al. [20] proposed an adaptive anchor and global context (GC) module for meter detection, which combines deep learning methods and traditional computer vision methods to achieve power equipment meter recognition. The above methods adopt the deep learning method in the instrument detection stage but are not applied to the identification of pointer and scale, resulting in limited improvement of reading robustness.

Compared to meter detection, reading recognition is a more complex task. Especially for such tasks as patrol robot automatic meter reading, the scene of the image to be identified usually has a large difference due to background changes, robot movement, and other factors. The focus of research is to stably recognize the dial information of meters for reading under different conditions. The deep learning-based image segmentation technology has been applied to detect scales and pointers, leading to a significant improvement in the robustness of the reading system. Alexeev et al. [21] proposed a three-level model to regress the coordinates of the keypoints in the panel but did not investigate the pointer recognition and reading strategies. Zuo et al. [22] improved Mask-RCNN to extract binary marks of the instrument dial and pointer. In [23], a modified RFB-Net network was used to detect the keypoint of the pointer image. Dong et al. [24] developed a vector detection network to recognize the direction of the pointer. Compared to traditional methods, these CNN-based pointer and dial detection methods greatly reduced the probability of missed detection and false detection, enabling the recognition of various analog meters in dynamic scenes. However, no optimal general reading method exists for the many types of analog meters for electric power and pressure measurement. Deng et al. [25] proposed a meter reading method that combines YOLOv5s and DeeplabV3+ networks. The segmented dashboard area is unfolded, and the reading is calculated by calculating the distance between the pointer and the scale. Zhou et al. [26] proposed an end-to-end pointer meter reading method based on deep learning. Simultaneously locate the pointer and extract the pointer object and achieve meter reading recognition through the local angle method. These reading methods, which also apply deep learning technology in the reading stage after the dial detection and positioning, have achieved good results in terms of reading accuracy and robustness. But training a model that can segment all the scale and pointer information on the dial requires a large amount of annotated data. And it requires a more complex post-processing process to determine the relationship between the pointer and the scale.

The acquired meter images may be blurred and distorted due to environmental factors and the robot's motion factors [27]. It is better to use image quality assessment to filter out the images with good imaging effects for reading recognition. Image quality assessment methods are categorized into subjective and objective assessment. Objective assessment methods give a quantitative result based on a mathematical model. A well-designed objective assessment method can be very close to the subjective judgment of a human being. It can effectively screen out images with more distinctive features for further processing before detection.

In this study, a fast-reading method based on object and keypoint detection is proposed to read analog meters for inspection robots in motion. Our reading method consists of a target detection model and a keypoint detection model. First, a YOLOv5s [28] target detection network is used to detect analog meters in complex patrol scenes. Second, inspired by the human posture estimation algorithm, the High-Resolution Net (HRNet) [29] is used to extract the scale and pointer information of the detected analog meter panel. Third, the objective image quality assessment method is used to evaluate the meter images collected by inspection robots, and the best quality images are selected for reading calculation. Finally, based on the results of instrument target detection and keypoint detection, the reading is calculated by the angle of the pointer.

The primary contributions of our study are as follows.

1. The YOLOv5s network is used for instrument detection, which is suitable for the complex working scene of patrol robots.
2. A keypoint detection method is used for the detection of analog meter range and pointer, which improves the reading recognition effect.
3. A meter recognition method for inspection robots in motion is proposed, which selects the best quality image from consecutive frames of the video stream and accurately recognizes circular simulated meter readings.

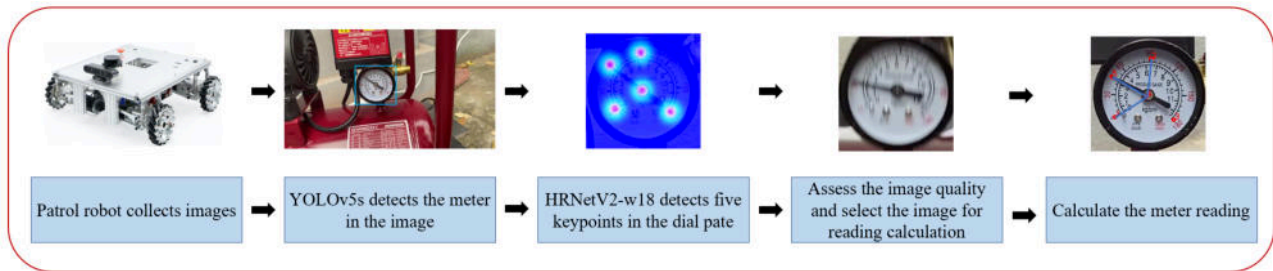


Fig. 2.1: Flowchart of the proposed reading method.

4. The effect of the proposed reading method is verified on the real inspection robot platform.

2. Proposed Method. We propose a deep learning-based method for fast meter reading. Fig. 2.1 illustrates its flowchart. First, the inspection robot performs analog meter target detection under the moving state. Real-time video data can be processed directly through the Nvidia Jetson edge computing device mounted on the robot. Or transmit it to the computer for processing through network streams such as RTSP and RTMP. The YOLOv5s detection model is used to detect and mark the pointer meters in the field of view of the inspection robot in real-time. Second, inspired by the method of human posture estimation, the HRNet network is modified to detect five keypoints in the dashboard: the start and end of the range, the midpoint of the range, the center of the dial, and the end of the pointer. Third, an objective image quality assessment method that combines information entropy, standard deviation, and the mean gradient is used to select the optimal quality image for reading recognition. Finally, a method based on pointer deflection angle calculation was used for meter reading recognition.

2.1. Analog Meter Detector Based on Yolov5s. The key to accurately reading a pointer instrument is to identify and locate the instrument panel area in the image. It is almost impossible for the traditional target detection method to recognize the instrument panel stably and accurately under the complex and changeable image background conditions collected by the inspection robot. The target detection method based on deep learning makes this application possible. The target detection algorithm can be divided into two types: one-stage method and two-stage method. The one-stage method represented by YOLO [30] has high real-time performance, but it is usually slightly inferior to the recognition accuracy of the two-stage target detection method.

YOLO (You Look Only Once) is a one-stage target detection method that predicts bounding boxes and class probabilities directly from an input image. YOLOv5s has the smallest network depth and the smallest feature map width among four variants: YOLOv5s, YOLOv5m, YOLOv5l, and YOLOv5x. It is mainly composed of input, backbone, neck, and prediction. The input part enriches the data set by splicing training data to achieve a better detection effect with smaller samples. The backbone part is mainly composed of a Cross Stage Partial (CSP) module for feature extraction. Feature Pyramid Network (FPN) and Path Aggregation Network (PANet) are used in the neck part to aggregate the image features preliminarily extracted from the backbone part. The prediction part performs target prediction and outputs the prediction results.

The target detection of the analog meter using YOLOv5s mainly includes four steps. First, collect and label the training images with bounding boxes around pointers. Second, build the training set, validation set, and test set of YOLOv5s network according to a certain ratio. Third, train the target detection model using a deep learning framework with appropriate hyperparameters. Finally, test the model recognition effect by running inference on test set images and evaluating metrics such as precision and recall.

We use the mosaic data augmentation method to improve the accuracy of YOLOv5s target detection model with fewer labeled samples. This method randomly crops, rotates, scales, and color transforms four images, and then combines them into one image as a training input sample. It makes the scale and color space of the sample more variety, and makes the limited data generate more value. Figure 2.3 illustrates how mosaic data augmentation method improves the pointer meter data. This method helps the model learn from different

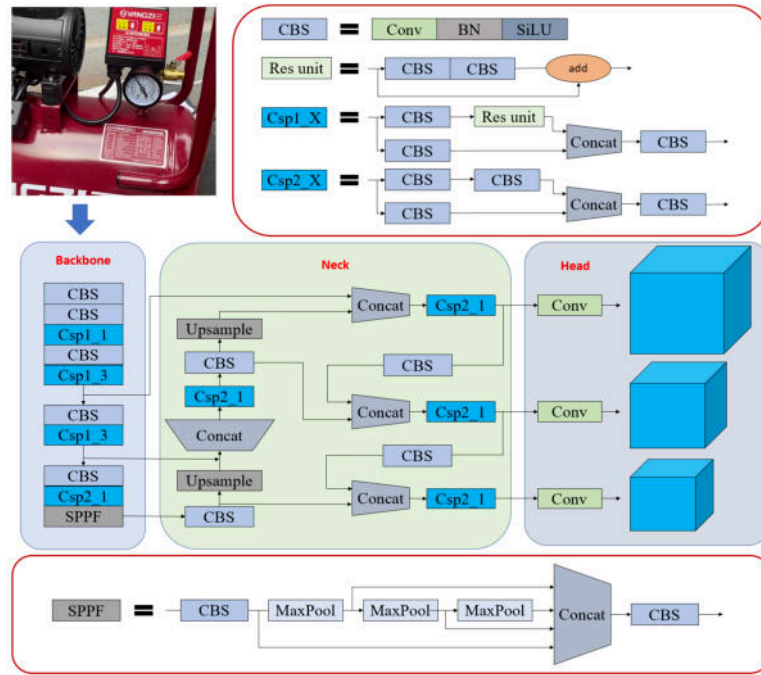


Fig. 2.2: The YOLOv5s framework.



Fig. 2.3: Mosaic data augmentation.

contexts and scales of the pointer meter images. It has been verified that this method can effectively enhance the model’s ability to generalize to unseen data.

For the robot that checks along the preset route, the pointer meter usually appears from one end of the captured image and disappears from the field of vision from the other end as the robot moves. Obviously, for the reading calculation of the pointer meter, the image collected when the camera is facing the instrument can get a more accurate reading. For each detected target, YOLOv5s outputs the coordinates of the upper left

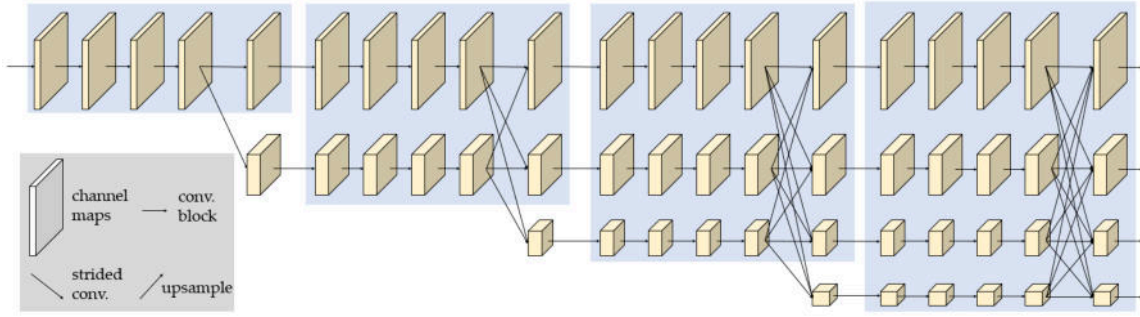


Fig. 2.4: Backbone structure of HRNet.

corner (x_1, y_1) and the lower right corner (x_2, y_2) of the bounding box to achieve the positioning of the pointer meter. R_p is calculated as shown in Equation (2.1). The relative position R_p of the center point of the bounding box in the whole image is used to determine the angle between the camera and the pointer instrument. The closer the R_p is to 0.5, the higher the alignment between the camera and the target pointer gauge.

$$R_p = \frac{x_2 + x_1}{2w} \quad (2.1)$$

where w represents the width of the whole image.

2.2. Keypoint Detector Based on HRNetV2-w18. When the instrument in the picture is detected, the most critical step is to identify the scale and pointer. We can use angle calculation or distance calculation methods for reading recognition of pointer instrument. These methods have different pros and cons. The distance calculation method needs higher accuracy of scale and pointer position recognition and gives higher reading accuracy, but it also demands higher quality of collected images. The angle calculation method is more robust and can be more precise even with unstable image quality.

HRNet is designed to preserve high-resolution features throughout the network by using multiple parallel branches with different resolutions. The structure of HRNet is shown in Figure 2.4. The branches are connected by repeated multi-scale fusion modules that allow information exchange across resolutions. HRNet has several variants with different depths and widths to suit different applications and resources. HRNetV2-w18 is a variant that has a smaller width than other versions. For inspection robots that need to read pointer meters while moving, detection speed and accuracy are crucial. The HRNetV2-w18 network can achieve a good balance between these two factors.

In the keypoint detection task, the position learning of key points can be divided into two categories: heatmap-based and region-based. The keypoints in the image cannot be represented by a single pixel, which may be composed of the labeled coordinates and some nearby pixels. If all the pixels except the marker coordinates are defined as negative samples, the model may be difficult to converge. We use the heatmap method to obtain higher coordinate prediction accuracy. The generation method of heat map is shown in Equation (2.2).

$$Heatmap(x, y) = e^{-\frac{(x-\mu_x)^2 + (y-\mu_y)^2}{2\sigma^2}} \quad (2.2)$$

where μ_x and μ_y represent the true keypoint coordinates obtained from annotation, and $Heatmap(x, y)$ is the value of a point (x, y) on the heatmap.

2.3. Objective Image Quality Assessment. We propose a reference-free image quality assessment method for images acquired by inspection robots. The calculated metrics include entropy, standard deviation and mean gradient. Entropy measures the amount of information contained in an image; higher information entropy indicates that the image contains more information, and the image is usually more detailed. The image



Fig. 2.5: Reading calculation methods in two cases: (a) The pointer is in the first half of the range; (b) The pointer is in the second half of the range.

is first converted to a gray level image and the probability of occurrence of each gray level is counted to finally get the information entropy. The entropy is calculated as shown in Equation (2.3).

$$H = - \sum_{i=0}^{255} p_i \log_2 p_i \quad (2.3)$$

where p_i is the probability of occurrence of the corresponding gray level.

The standard deviation reflects the degree of dispersion between the pixel values and the mean value of the image, and a larger standard deviation usually indicates a better image quality. The standard deviation is calculated as shown in Equation (2.4).

$$\sigma = \sqrt{\frac{1}{w * h} \sum_{i=1}^w \sum_{j=1}^h (p_{ij} - \mu)^2} \quad (2.4)$$

where w and h are the width and height of the image, p_{ij} is the pixel value of the corresponding coordinate and μ is the mean value of the image.

The mean gradient reflects the rate of change of the gray values on both sides of the image edges, this data can be used to measure the fineness of the image details, the larger the mean gradient is, the clearer the image is in general. The mean gradient is calculated as shown in Equation (2.5).

$$G = \frac{1}{w * h} \sum_{i=1}^w \sum_{j=1}^h \sqrt{\frac{\left(\frac{\partial f}{\partial x}\right)^2 + \left(\frac{\partial f}{\partial y}\right)^2}{2}} \quad (2.5)$$

where w and h are the width and height of the image, $\frac{\partial f}{\partial x}$ and $\frac{\partial f}{\partial y}$ are the gradients of the image horizontally and vertically.

We normalize the above three metrics by mapping them between 0 and 1. The number of our image dataset is small, and the normalization is performed by using between the maximum and minimum values. After actual testing, here we no longer assign different weights to the above three metrics, and use the score obtained by Equation (2.6) as the final assessment of image quality. In the application, images with meter alignment values R_p greater than 0.35 and less than 0.65 will be calculated for image quality, and the reading with the highest image quality score will be used as the reading for that meter.

$$Score = H + \sigma + G \quad (2.6)$$

2.4. Reading Calculation Based on Keypoints. Upon acquisition of precise dial scale and pointer end coordinates, determination of the rotation angle of the pointer enables computation of the reading of the meter. Figure 2.5 illustrates two distinct methods for computing the reading of the meter, which depend on the position of the pointer relative to the scale. If the pointer falls between the starting point and the midpoint of



Fig. 3.1: Examples of pointer meter annotations. (a) Instrument A with a maximum range of 180 Lb/in²; (b) Instrument B with a maximum range of 0.6 MPa; (c) Instrument C with a maximum range of 1.6 MPa.

the scale, the reading is determined using these two reference points. In contrast, if the pointer has surpassed the midpoint and is in closer proximity to the endpoint, the reading is calculated using the midpoint and endpoint of the scale.

In Figure 2.5(a), the position of the pointer falls within the initial half of the meter's range, whereby the vectors \overrightarrow{CS} and \overrightarrow{CM} , represented by points 4 and 1 and points 4 and 2 respectively, serve as the starting and ending points for the beginning and end of the range. To determine half of the full range of the meter, the angle α enclosed between the two vectors is computed. To calculate the meter reading, vector \overrightarrow{CP} is constructed using points 4 and 5 as the starting and ending points for representation of the pointer. The included angle β between vector \overrightarrow{CP} and \overrightarrow{CS} is then ascertained. The reading of the meter can be calculated using Equation (2.7).

$$Numf = \frac{90\alpha}{\beta} \quad (2.7)$$

In Figure 2.5(b), the pointer is situated in the second half of the range. The vector \overrightarrow{CM} with points 4 and 2 as the starting and ending points signifies the beginning range, whereas the vector \overrightarrow{CE} , represented by points 4 and 3, corresponds to the end of the range. Vector \overrightarrow{CP} , constructed with points 4 and 5, portrays the pointer. To determine the meter reading, the enclosed angles α and β between vector \overrightarrow{CP} and \overrightarrow{CM} , and \overrightarrow{CM} and \overrightarrow{CE} , respectively, are calculated. The reading of the meter can be calculated using Equation (2.8).

$$Nume = \frac{90(\alpha + \beta)}{\beta} \quad (2.8)$$

3. Experiments and Results.

3.1. Experimental Environment and Dataset. We ran the proposed algorithm on a computer with I7-13900H CPU, 32 GB RAM and NVIDIA GeForce RTX4060 8GB GPU. We used PyTorch deep learning framework, Python 3.10 programming language, CUDA 11.8 and cuDNN 8.9 NVIDIA acceleration tools.

We collected 1632 images of three kinds of air pressure pointer meters using an industrial camera with a resolution of 1920×1080 pixels. We labeled the images with LabelMe, an open-source annotation tool. The position of the pointer in the image and the five key points in the dial are marked at one time. The position of the pointer meter is marked with the bounding box. The start of the range is marked with 1, the midpoint of the range is marked with 2, the end of the range is marked with 3, the center of the dial is marked with 4, and the end of the pointer is marked with 5. Figure 3.1 shows examples of pointer meter annotations in the dataset.

The marked data is further processed to provide the YOLOv5s target detection model and HRNet key point detection model for training. The bounding box and category information marked by LabelMe software are extracted and stored in the format of VOC data set and provided to YOLOv5s model. The heatmap files, which are produced using the methodology outlined in Section 2.2, are provided to HRNetV2-w18 for training a keypoint detection model. Table 3.1 shows the number of different keypoints marked on the pointer meter.

Table 3.1: Definition of keypoints of the meter.

Label number	Position of the pointer meter
1	The start of the range.
2	The midpoint of the range.
3	The end of the range.
4	The center of the dial.
5	The end of the pointer.

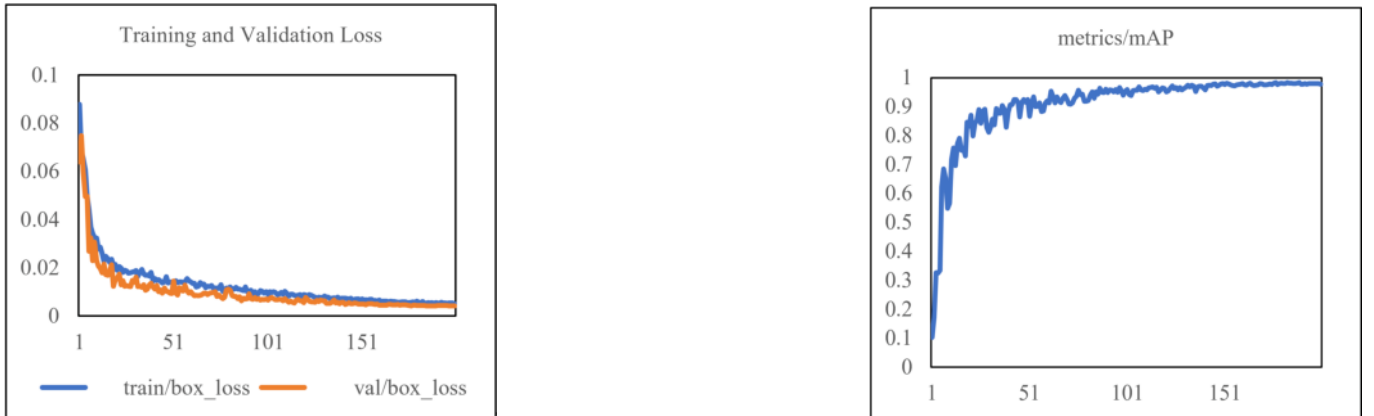


Fig. 3.2: Loss and mAP variation curves. (a) The loss variation curves for the training and validation sets; (b) mAP variation curve.

3.2. Experimental Results.

3.2.1. YOLOv5s Analog Meter Detector. The dataset was partitioned into three subsets, namely training, validation, and testing, in an 8:1:1 ratio. We trained YOLOv5s model with an input image resolution of 640×640 pixels, a batch size of 8, an initial learning rate of 0.001, and a training duration of 200 epochs. Due to the small size of the dataset, we utilized a pre-trained model on the COCO dataset provided by the official source to initialize the weights of our model, aiming to achieve better recognition performance. Figure 3.2(a) and Figure 3.2(b) illustrate the variation of loss and mean average precision (mAP) during the training process of the YOLOv5s object detection model. From Figure 3.2(a), it can be observed that the loss for both the training and validation datasets gradually decreases as the training progresses. After the 150th epoch, the loss stabilizes. Figure 3.2(b) presents that the model achieves a high mAP of 98.3% at last.

On the self-built pointer instrument dataset, YOLOv5s was compared with other common models. The training parameter settings remained unchanged from the previous text. The performance of the optimal weight of each model on the test set is shown in Table 3.2, and YOLOv5s achieves a balance between accuracy and detection speed. The average accuracy has reached 97.9%, and the detection speed can reach 33.78 FPS.

3.2.2. HRNetV2-w18 Keypoint Detector. The circular meter area in the image is obtained by the target detector and adjusted to 384×384 pixels before being input into the HRNetV2-w18 keypoints detection model. The batch size is set to 1, and stochastic gradient descent (SGD) is used for parameter optimization with an initial learning rate of $1e-5$ over a total training epoch of 60. The network outputs are heatmaps, and the network's keypoints detection performance is evaluated using root mean square error (RMSE) after extracting keypoints. Figure 3.3(a) and Figure 3.3(b) show the changes in loss on the training and validation sets during the HRNetV2-w18 training process. It can be seen that after the 100th epoch, the loss basically does not decrease, and the training is completed.

Table 3.2: Comparison of YOLOv5s with Faster R-CNN, SSD and PP-YOLOE-s on the test dataset.

Method	Epochs	mAP	FPS
Faster RCNN	200	0.975	6.71
SSD	200	0.925	26.96
PP-YOLOE-s	200	0.749	18.21
YOLOv5s	200	0.979	33.78

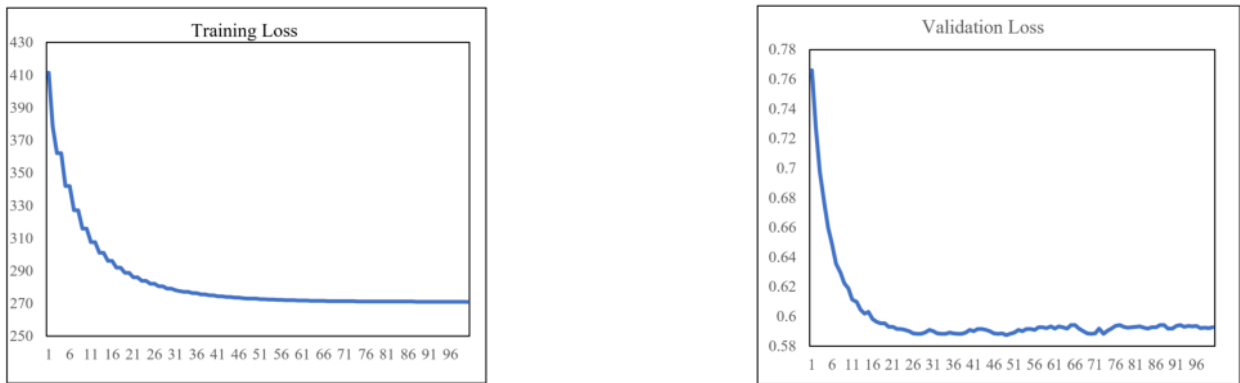


Fig. 3.3: The loss curve of the training and validation sets during the training process. (a) The loss variation curves for the training sets; (b) The loss variation curves for the validation sets.

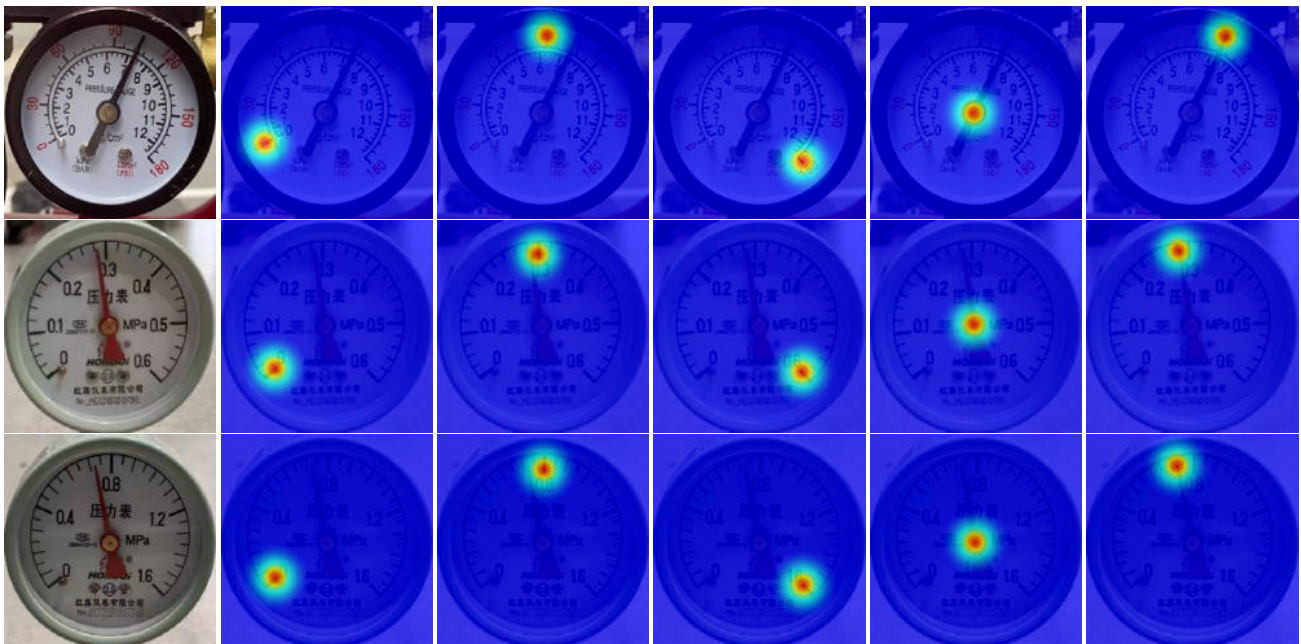


Fig. 3.4: Keypoint detection results. (a) Cropped and resized pointer instrument image detected by YOLOv5s;(b-f) Predicted heatmaps for 5 keypoints.

Table 3.3: Maximum and minimum values of image quality metrics for the dataset.

Image quality metric	Maximum value	Minimum value
Entropy	7.785	5.618
Standard deviation	78.967	13.184
Mean gradient	89.982	7.815

Table 3.4: Maximum and minimum values of image quality metrics for the dataset.





Num.	Image	Entropy	Standard deviation	Mean gradient	Score
1		0.458	0.228	0.126	0.812
2		0.470	0.274	0.190	0.934
3		0.486	0.200	0.310	0.996
4		0.563	0.352	0.359	1.274

Figure 3.4 shows the detection results output by the HRNetV2 w18 model, and the predicted results of the five key points are presented in heatmaps. For three different dial types of pressure gauges, the model can accurately locate the key points of the readings. The key point positions selected by this method have relatively universal characteristics.

3.2.3. Image Quality Assessment. The evaluation method established in the previous section is used to select the image with the best image quality for meter reading recognition. The three metrics of entropy, standard deviation and mean gradient are calculated for all images in the image dataset and their maximum and minimum values are shown in Table 3.3. It can be seen that the contribution of the entropy metrics to the final score may not be fully reflected if normalization is not performed. It can be seen that the contribution of the entropy to the final score may not be fully reflected if normalization is not performed. When the dataset is large enough, the weights of the three metrics' contribution to the final score can be further assigned. Here we take the normalized three metrics and add them directly.

Table 3.4 gives the images captured while the inspection robot is moving, and their image quality is evaluated after locating and intercepting the meter dial area images. Higher values of the three image quality metrics and assessment scores indicate better image quality.

3.2.4. Meter Reading Recognition. After detecting the keypoint on the dial of the pointer meter, the reading of the meter can be calculated using the method proposed in Section 2.4. This angle-based reading calculation method has a significant impact on the calculation accuracy by the positioning accuracy of keypoints. Especially when the deviation degree of the center point detection of the dial is relatively high, it will bring significant errors to the reading calculation. However, compared to other pointer meter reading methods based on semantic segmentation, using reading methods based on key points and angles has lower data annotation costs. Adding half range key point annotation will not excessively increase the cost of data annotation but can to some extent improve reading accuracy.

Table 3.5: Reading error of different strategies.

Num.	Ground truth	Full range angle reading results	E_{RF}	Half range angle reading results	E_{RH}
1	30.0	26.8	10.67 %	31.8	6.00%
2	46.8	44.2	5.56%	44.5	4.91%
3	62.4	64.7	3.69%	65.2	4.49%
4	68.4	72.1	5.41%	71.1	3.95%
5	91.2	91.9	0.77%	90.4	0.88%
6	103.2	106.7	3.39%	101.1	2.03%
7	105.6	102.0	3.41%	107.9	2.18%
8	124.8	131.5	5.37%	119.6	4.17%
9	0.168	0.181	7.74%	0.151	10.12%
10	0.204	0.213	4.41%	0.199	2.45%
11	0.284	0.288	1.41%	0.290	2.11%
12	0.340	0.365	7.35%	0.358	5.29%
13	0.392	0.385	1.79%	0.393	0.26%
14	0.466	0.483	3.65%	0.480	3.00%
15	0.26	0.29	11.54%	0.25	3.85%
16	0.56	0.62	10.71%	0.59	5.36%
17	0.70	0.71	1.43%	0.73	4.29%
18	0.92	0.98	6.52%	0.96	4.35%
19	0.99	0.95	4.04%	1.02	3.03%
20	1.18	1.11	5.93%	1.22	3.39%

The comparison between the reading results and the true values using the method presented in this article is shown in Table 3.3. The true value is obtained by manually observing the instrument horizontally from the front. Evaluate the effectiveness of the proposed method by calculating the error between the automatic reading and the actual reading. The calculation formula for reading error E_R is shown in Equation (3.1).

$$E_R = \frac{|T - L|}{T} \times 100\% \quad (3.1)$$

where L is the value obtained by the proposed automatic reading method, and T is the instrument reading obtained through manual observation.

We calculated the readings obtained based on the full range key points and the readings obtained based on the half range keypoints. Then evaluate the accuracy of the readings by calculating their errors using true values. The decimal places of manually observed values are calculated based on 1/5 of the pressure gauge graduation value. Table 3.5 shows the reading error results obtained by different strategies under the same keypoint detection results.

The different angles at which inspection robots collect analog meter images can have an impact on the reading results. The instrument images used for calculating readings in the experiment are collected with the camera horizontally centered on the analog meters. From the results shown in Table 3.3, it can be seen that the reading strategy using half range key points has higher accuracy. From the results shown in Table 3.3, it can be seen that the reading strategy using half range key points has higher accuracy.

4. Discussion. This article proposes a pointer instrument reading method based on key point recognition, inspired by the top-down human posture estimation method. It consists of a target detector and a keypoint detector. This detection method has high accuracy, but its computational complexity increases linearly with the increase of multiple targets in the image. For the application of patrol robots, the accuracy advantage of this method is more prominent. The light target detection network based on YOLOv5s achieves the balance between detection speed and accuracy. It can be easily transplanted to the edge computing equipment carried by the patrol robot. A reading calculation method based on five key point detection can achieve high reading accuracy through finetune with a small amount of annotated data.

However, this is not an end-to-end recognition method. In the future, pointer instrument reading recognition may use multitask learning methods. It can use the network to simultaneously perform object detection and keypoint detection, share the same feature extraction backbone, and improve computational efficiency. To recognize readings from different kinds of meters in the future, the proposed method should also account for pointer meters' range recognition. The meter's measuring range can be either pre-entered as prior knowledge for different types or detected from the digits on the dial.

REFERENCES

- [1] Jaffery, Z.A.; Dubey, A.K. Architecture of noninvasive real time visual monitoring system for dial type measuring instrument. *IEEE Sensors Journal* **2012**, *13*, 1236-1244.
- [2] Zhang, J.; Ge, K.; Xun, L.; Sun, X.; Xiong, W.; Zou, M.; Zhong, J.; Li, T. MFCD-Net: Cross Attention Based Multimodal Fusion Network for DPC Imagery Cloud Detection. *Remote Sensing* **2022**, *14*, 3905.
- [3] Gao, H.; Yi, M.; Yu, J.; Li, J.; Yu, X. Character segmentation-based coarse-fine approach for automobile dashboard detection. *IEEE Transactions on Industrial Informatics* **2019**, *15*, 5413-5424.
- [4] Liu, L.; Qiao, X.; Liang, W.-z.; Oboamah, J.; Wang, J.; Rudnick, D.R.; Yang, H.; Katimbo, A.; Shi, Y. An Edge-computing flow meter reading recognition algorithm optimized for agricultural IoT network. *Smart Agricultural Technology* **2023**, *5*, 100236.
- [5] Chen, Y.-S.; Wang, J.-Y. Computer Vision-Based Approach for Reading Analog Multimeter. *Applied Sciences* **2018**, *8*, 1268.
- [6] Zou, L.; Wang, K.; Wang, X.; Zhang, J.; Li, R.; Wu, Z. Automatic Recognition Reading Method of Pointer Meter Based on YOLOv5-MR Model. *Sensors* **2023**, *23*, 6644.
- [7] Guo, X.; Zhu, Y.; Zhang, J.; Hai, Y.; Ma, X.; Lv, C.; Liu, S. Intelligent pointer meter interconnection solution for data collection in farmlands. *Computers and Electronics in Agriculture* **2021**, *182*, 105985.
- [8] Alegria, E.C.; Serra, A.C. Automatic calibration of analog and digital measuring instruments using computer vision. *IEEE transactions on instrumentation and measurement* **2000**, *49*, 94-99.
- [9] Hou, L.; Qu, H. Automatic recognition system of pointer meters based on lightweight CNN and WSNs with on-sensor image processing. *Measurement* **2021**, *183*, 109819.
- [10] Li, D.; Li, W.; Yu, X.; Gao, Q.; Song, Y. Automatic Reading Algorithm of Substation Dial Gauges Based on Coordinate Positioning. *Applied Sciences* **2021**, *11*, 6059.
- [11] Li, Z.; Zhou, Y.; Sheng, Q.; Chen, K.; Huang, J. A high-robust automatic reading algorithm of pointer meters based on text detection. *Sensors* **2020**, *20*, 5946.
- [12] Cai, W.; Ma, B.; Zhang, L.; Han, Y. A pointer meter recognition method based on virtual sample generation technology. *Measurement* **2020**, *163*, 107962.
- [13] Laroca, R.; Barroso, V.; Diniz, M.A.; Gonçalves, G.R.; Schwartz, W.R.; Menotti, D. Convolutional neural networks for automatic meter reading. *Journal of Electronic Imaging* **2019**, *28*, 013023-013023.
- [14] Li, T.; Meng, Z.; Ni, B.; Shen, J.; Wang, M. Robust geometric ℓ_p -norm feature pooling for image classification and action recognition. *Image and Vision Computing* **2016**, *55*, 64-76.
- [15] Zhang, C.; Shi, L.; Zhang, D.; Ke, T.; Li, J. Pointer Meter Recognition Method Based on Yolov7 and Hough Transform. *Applied Sciences* **2023**, *13*, 8722.
- [16] Zhang, Z.; Hua, Z.; Tang, Y.; Zhang, Y.; Lu, W.; Dai, C. Recognition method of digital meter readings in substation based on connected domain analysis algorithm. *Actuators* **2021**, *10*, 170.
- [17] Huang, J.; Wang, J.; Tan, Y.; Wu, D.; Cao, Y. An automatic analog instrument reading system using computer vision and inspection robot. *IEEE Transactions on Instrumentation and Measurement* **2020**, *69*, 6322-6335.
- [18] Liu, Y.; Liu, J.; Ke, Y. A detection and recognition system of pointer meters in substations based on computer vision. *Measurement* **2020**, *152*, 107333.
- [19] Salomon, G.; Laroca, R.; Menotti, D. Image-based automatic dial meter reading in unconstrained scenarios. *Measurement* **2022**, *204*, 112025.
- [20] Fan, Z.; Shi, L.; Xi, C.; Wang, H.; Wang, S.; Wu, G. Real time power equipment meter recognition based on deep learning. *IEEE Transactions on Instrumentation and Measurement* **2022**, *71*, 1-15.
- [21] Alexeev, A.; Kukharev, G.; Matveev, Y.; Matveev, A. A highly efficient neural network solution for automated detection of pointer meters with different analog scales operating in different conditions. *Mathematics* **2020**, *8*, 1104.
- [22] Zuo, L.; He, P.; Zhang, C.; Zhang, Z. A robust approach to reading recognition of pointer meters based on improved mask-RCNN. *Neurocomputing* **2020**, *388*, 90-101.
- [23] Zhang, Q.; Bao, X.; Wu, B.; Tu, X.; Jin, Y.; Luo, Y.; Zhang, N. Water meter pointer reading recognition method based on target-key point detection. *Flow Measurement and Instrumentation* **2021**, *81*, 102012.
- [24] Dong, Z.; Gao, Y.; Yan, Y.; Chen, F. Vector detection network: An application study on robots reading analog meters in the wild. *IEEE Transactions on Artificial Intelligence* **2021**, *2*, 394-403.
- [25] Deng, G.; Huang, T.; Lin, B.; Liu, H.; Yang, R.; Jing, W. Automatic meter reading from UAV inspection photos in the substation by combining YOLOv5s and DeepLabv3+. *Sensors* **2022**, *22*, 7090.
- [26] Zhou, D.; Yang, Y.; Zhu, J.; Wang, K. Intelligent reading recognition method of a pointer meter based on deep learning in a real environment. *Measurement Science and Technology* **2022**, *33*, 055021.
- [27] Wu, X.; Shi, X.; Jiang, Y.; Gong, J. A high-precision automatic pointer meter reading system in low-light environment.

- Sensors* **2021**, *21*, 4891.
- [28] Jocher, G.; Stoken, A.; Borovec, J.; Changyu, L.; Hogan, A.; Chaurasia, A.; Diaconu, L.; Ingham, F.; Colmagro, A.; Ye, H. ultralytics/yolov5: v4. 0-nn. SiLU () activations, Weights & Biases logging, PyTorch Hub integration. Zenodo **2021**.
- [29] Sun, K.; Xiao, B.; Liu, D.; Wang, J. Deep high-resolution representation learning for human pose estimation. *In Proceedings of the IEEE/CVF conference on computer vision and pattern recognition*, **2019**; pp. 5693-5703.
- [30] Yin, H.; Chen, M.; Fan, W.; Jin, Y.; Hassan, S.G.; Liu, S. Efficient Smoke Detection Based on YOLO v5s. *Mathematics* **2022**, *10*, 3493.

Edited by: Bradha Madhavan

Special issue on: High-performance Computing Algorithms for Material Sciences

Received: Dec 6, 2023

Accepted: Feb 16, 2024